JOURNAL OF SOLID STATE CHEMISTRY 25, 367–378 (1978)

Chemical Diffusivity and Electrical Conductivity in TiO_2 Containing a Submicron Dispersion of SiO_2

G. M. CROSBIE*

Department of Materials Science and Engineering and Materials Research Center, Northwestern University, Evanston, Illinois 60201

Received November 15, 1977; in revised form February 6, 1978

Owing to the electrically charged nature of crystal defects in oxides, the possibility exists to reduce diffusivity with a two-phase microstructure of sufficiently small dimensions. A diminution of the order of 10 times in the chemical diffusivity at 1153°C has been repeatedly observed in polycrystalline rutile with an initial second-phase particle size of about 50 Å. The dependence of the diffusivity and electrical conductivity upon particle size and volume fraction is explained in terms of the alteration of concentrations of transport-related point defects by the transfer of charged species to internal surfaces.

Introduction

Advances which have been made in understanding the effects of elements in solution in oxides have had far-reaching implications for applications of materials with both high and low rates of transport of electrons and ions. Relatively little work, though, has been done on elements present out of solution, as, for example, with dispersed phases of controlled volume fraction and particle size. Recently, unusually low mass transport has been observed in oxides with submicron dispersions of second phases. Particularly notable is the observation of a marked reduction in oxidation rate of chromia scale forming alloys caused by the addition of a few volume percent of a dispersion of particles less than 500 Å in size (*1*, *2*). The classical theory of series-parallel conductivity and diffusivity (*3*, *4*) cannot explain the size dependence and magnitude of the change. In the particular cases of the ionic conducting compounds LiI (*5*) and CuCl (*6*), a dispersion of an insulating second phase increases conductivity markedly. For these cases, the classical theory cannot even explain the direction of change.

Experimental

Two-phase billets with volume fractions of SiO_2 from 0 to 0.1 were prepared (on the basis of rutile density of 4.26 g/cm^3 and SiO_2 density of 2.32 g/cm^3) from ultrafine powders which had been produced by hydrolysis of the respective tetrachlorides (*7*). Interdispersion was obtained by mechanical shearing and ultrasonic agitation in a deionized water slurry. The water was removed by freeze-drying. The powder was consolidated by ceramic hot pressing in loose graphite dies under vacuum. The looseness of the dies apparently (as checked by ir spectrophotometry) allowed outgassing of adsorbed water at time-temperature plateaus at 200 and 650°C before the compaction run to 1200°C for 1 h at 3500 psi and subsequent hot ejection.

* Present address: Pfizer, Inc., Minerals, Pigments & Metals Division, 640 N. 13th St., Easton, Pa 18042.

0022–4596/78/0254–0367$02.00/0

Bar samples of nearly square cross section were cut with a diamond wheel from the hot pressed billets. At least three bars were cut of each composition: one to supply samples of the microstructure as it changes with time at temperature and two for four-probe dc conductivity tests with cross-sectional areas differing by a factor of 10. The bars were given a uniform finish in the conductivity gauge length by dry grinding on SiC papers up to 500 grit. The grinding was followed by acetone and ethanol rinses.

Pt electrodes were held in place by shallow notches in one face of each bar, by crimping, and by the cohesion of unfluxed platinum paste. The minimum spacing between any two of four electrodes was three times the bar thickness. Typically, the thick and thin conductivity bars were run simultaneously. Each bar was connected by its electrodes to an alumina cage or frame in a 1-in. alumina core in a tube furnace. The bars were mounted directly above $\frac{1}{8}$-in. ports in the mullite space disks of the frame, through which the preheated gas mixture flowed upward. From time to time, samples for microstructure were withdrawn from the bottom of the furnace.

A Keithley 225 constant current source and a Fluke 8200 A digital dc millivoltmeter were used for the conductivity measurements. Current reversal was obtained with Grigsby–Barton diode-locking relays controlled by signals from a Data General Nova 1220 minicomputer, which was in turn interfaced to the digital voltmeter. Currents and voltages consistently checked to better than $\frac{1}{2}$% against standard resistors and cells. The computer interaction facilitated handling of the large volume of bar conductivities which were routinely collected and analyzed for chemical diffusivity after each step-like change in atmosphere. The analysis used here is similar to that of Price and Wagner (*8*). The numerical factors appropriate to thin bars of square section are listed in Table I.

A solid state proportional controller was used with a constant voltage power supply.

TABLE I

NUMERICAL FACTOR RELATING PERCENTAGE CHANGE IN CONDUCTIVITY OF A THIN BAR OF SQUARE CROSS SECTION TO DIFFUSIVITY[a]

Percentage change	Dt/a^2 from (*8*)[b] (limiting case)	Present numerical calculation of Dt/a^2
58	—	0.132
70	—	0.198
79.2	—	0.271
89	—	0.401
90	0.339	0.420
92	0.385	0.465
95	0.480	0.560
96	0.525	0.605
98	0.666	0.746
99	0.806	0.886

[a] The mathematical solution to the boundary value problem corresponding to the sudden change in oxygen pressure at the surface of an infinitely long bar of square cross section can be expressed as an infinite series for each element of area in the section. The conductivity of the bar specimen corresponds to the average conductivity over the elements in the section because the conductivities add in parallel. In semi-ionic compounds, the ionic defect concentration (and therefore the ion diffusivity in simple cases) can be linearly related to electronic defect concentration (and conductivity). Thus, the diffusivity from this experiment represents the ion diffusivity in a chemical gradient, which is defined as the chemical diffusivity $\tilde{D}$. A numerical factor is required to relate percentage change in conductivity to specimen size, the time to reach a particular percentage change, and the chemical diffusivity. Price and Wagner (*8*) integrated using the first term of the series solution. The present numerical calculation used four terms. It is observed that the two solutions tend to converge in the limit of 100% change.

[b] Calculated by letting the square-side length $a = b$ and $c \to \infty$ from (*8*).

The specimen Pt–10Rh thermocouple was used as the input to the set-point controller.

The partial pressure of oxygen was controlled by a two-stream constant-head capillary drop flowmeter which was adapted from the design of Schwerdtfeger and Turkdogan (*9*). The design is adapted so that an electrical signal can cause the flow in one stream to drop to a second set-point while the flow in the

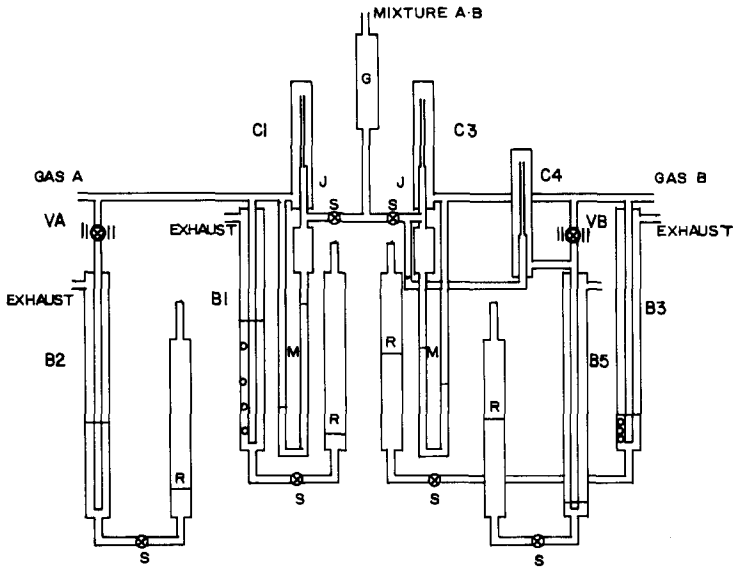

FIG. 1. Apparatus to control the gas mixing ratio with a constant total flow rate. When the solenoid valves VA and VB are opened, the flow rate of gas A decreases and the flow rate of gas B increases. When the solenoid valves are closed, the flow rate of gas A is fixed by the constriction of the capillary C1 and the pressure drop between the bubbler B1 and the gas mixing chamber G. Likewise, the flow rate of gas B is fixed by the constriction C3 and the pressure drop between B3 and G. When the valves VA and VB are opened, gas begins to bubble at points B2 and B5, rather than B1 and B3. Since there is a smaller pressure drop with the same capillary for gas A, the flow rate of gas A is reduced. While there is also a smaller pressure drop for gas B, a second capillary C4 is added in parallel, permitting the total flow through capillaries C3 and C4 to be greater. Other symbols denote S—stopcock; M—manometer; R—reservoir of hydraulic fluid; and J—a standard glass fitting. Adapted from Schwerdtfeger and Turkdogan (*9*).

other increases, thereby permitting a constant overall flow rate (about 0.5 cm/sec in a 1-in. tube with room temperature) with a different flow ratio of input gases. The design is shown in Fig. 1.

The bars were first equilibrated with a fixed oxygen pressure. Equilibrium was assumed complete when no further change in conductivity with time was observed. Then the oxygen pressure was suddenly changed to a new value and the conductivity was measured as a function of time.

Results

The chemical diffusivity calculated from 90 and 95% change in the conductivity of thick bar specimens (recorded during intraphase oxidations from 0.02 to 0.42 atm) is shown as a function of time in Fig. 2. For annealing times of less than 2×10^5 sec, the values for all the dispersed phase specimens are far below the values for specimens without a dispersion. Differences among the $\tilde{D}$'s appear in the sequence of volume fractions with the lowest diffusivity observed for the 10 vol% SiO_2 specimen. The lowest values are at least somewhat affected by the limit of the measurement as performed. A specimen of cross section, 0.3 $\times$ 0.3 cm, which is typical of the thick specimens used here, with 95% change in conductivity in 1500 sec (the time of each run) would yield a value of 3.3×10^{-5} cm^2/sec using the Dt/a^2 values of Table I. The diffusivity values obtained from transients recorded for thin bars would fall lower than the points plotted as the limit of the experiment is lower for thin bars which have $a = 0.1$ cm, rather than $a = 0.3$ cm.

The chemical diffusivity measured in a

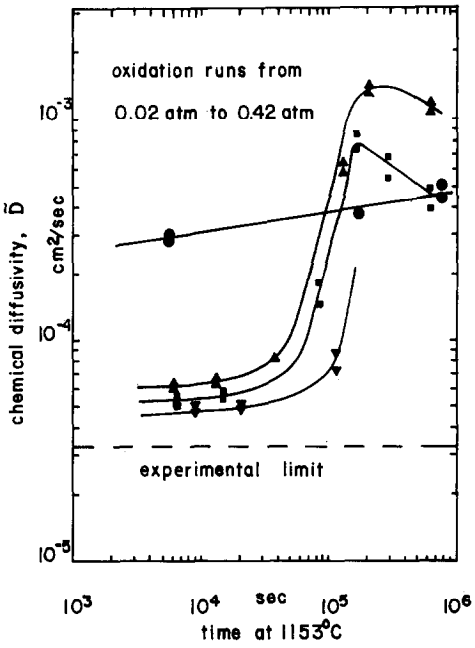

FIG. 2. Chemical diffusivity measured in $TiO_2(SiO_2)$ in switching from $P_{O_2} = 0.02$ atm to $P_{O_2} = 0.42$ atm as a function of annealing time. A straight-line is fit to the data for a specimen with no dispersed phase. Volume fractions are ● = 0; ▲ = 0.005; ■ = 0.02; and ▼ = 0.1. Data for specimens with dispersed phases are much lower than the data for a dispersion-free specimen for time shorter than 2×10^5 sec (about 3 days). The increase with time can be related to the microstructure through Eqs. (2*), (3*), and (4).

specimen without any dispersed phase increased from 2.8×10^{-4} cm²/sec to 4.4×10^{-4} cm²/sec during 9 days at 1153°C. The absolute value is roughly consistent with a value "of the order of 10^{-4} cm²/sec" reported by Baumard (*10*) for transient measurements on single crystal rutile in the more complex geometry of a van der Pauw cell at 1127°C. That the chemical diffusivity is so much higher than the ion diffusivities (estimated for 1153°C to be $D_{Ti} = 2.3 \times 10^{-11}$ cm²/sec from the work of Venkatu and Poteat (*11*), (presumably near 0.2 atm O_2 from the experimental method description) and $D_O = 1.2 \times 10^{-12}$ cm²/sec from the work of Haul and Dümbgen (*12*) (in the range from 0.08 to 1.6 atm)) is a result of the magnitude of the thermodynamic factor (T.F.) for a nearly stoichiometric compound. One estimate has been made (*13*) as $5/(2y)$ where y is the nonstoichiometry index in $Ti_{1+y}O_2$, with a value of 3×10^6 near 1 atm at 1153°C. The product of T.F. and the ion diffusivities then yields a value of the order of 10^{-4} cm²/sec for the chemical diffusivity which is nearly that of the presently measured $\tilde{D}$.

While transient data were recorded in regimes from 10^{-6} to 1 atm with argon–oxygen mixtures and with CO_2/CO ratios from 4 to 1600, only the switches between gases of most equal flow rates (high P_{O_2} with $Ar–O_2$ and low P_{O_2} with CO_2/CO) demonstrated differences of two and three times between thick and thin specimens to reach the same percentage change in conductivity. This is a consequence of the longer deadtime required to change the furnace atmosphere with a low flowrate component in the mixture. Thus, fewer diffusivities than conductivities can be discussed. Of those experiments that remain valid tests of bulk diffusivity, rather than tests of the deadtime, it was seen that the chemical diffusivity is lower in the low CO_2/CO range than in the near 1-atm range by a factor of 10. In the span between the two ranges, the conductivity increases by about 1000 times. Then, by comparison, the variation of $\tilde{D}$ with P_{O_2} is one of relatively little change, as has been cited by Baumard (*10*). The small change in $\tilde{D}$ with P_{O_2} is consistent with a thermodynamic factor which varies inversely with nonstoichiometry. The experimental activation energy in the range 1100 to 1200°C for the range of P_{O_2}'s from CO_2/CO to $Ar–O_2$ gives values calculated (without consideration of possible instrumental interference) between 18 and 33 kcal/mole (0.77 to 1.42 eV), on the basis of an observed increase of $\tilde{D}$ of about two times. The low activation energy is consistent with interstitial diffusion but is not consistent with the ion diffusion activation energies of about 60 kcal/mole of (*11*) and (*12*).

The equilibrium electrical conductivity of

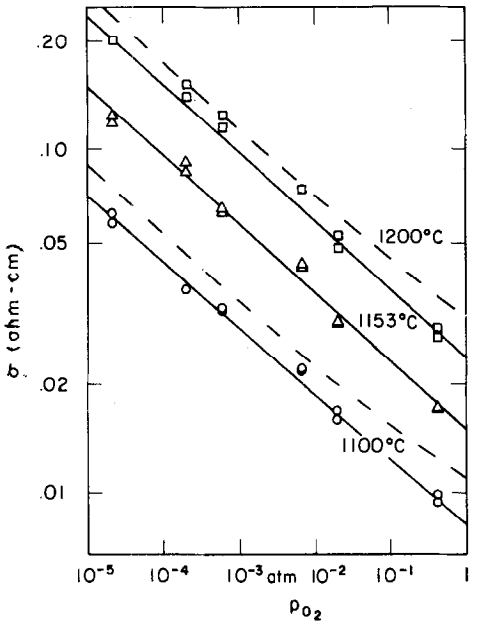

FIG. 3. Oxygen pressure dependence of TiO_2 conductivity. O = 1100°C; △ = 1153°C; and □ = 1200°C. The straight-lines are fits to the present experimental data. The value of the quotient $(\partial \ln \sigma / \partial \ln P_{O_2})$ is −0.199. The dashed curved lines near the 1100 and 1200°C data are the best-fit curves of (*14*) for a defect model of triply and quadruply ionized titanium interstitials.

TiO_2 with no dispersed phase is compared to the single-crystal *c*-axis conductivity of Blumenthal *et al.* (*14*) in the near-stoichiometry regime; see Fig. 3. Absolute values of conductivity fall about 20% below the values of the single-crystal work cited, but both sets of data appear to share the same slope in a plot versus P_{O_2}. It may be noted that the match extends to the CO_2/CO range studied. The purity of the TiO_2 was estimated from the mass spectrometric analysis (Table II) of material with 2 vol% of dispersed phase. The experimental activation energy of 1.96 eV (45.3 kcal/mole) from 1100 to 1200°C compares well with the value of 1.9 eV of Blumenthal *et al.* (*14*) for the near 1-atm range. The dependence on P_{O_2} in the range 10^{-6} to 1 atm is −0.199, which is close to the exponent $-\frac{1}{5}$ for quadruply ionized Ti interstitials. It may be that charges on Fe and Al impurities (Table II) compensate for charges

TABLE II

SPARK SOURCE MASS SPECTROMETRIC ANALYSIS OF A SAMPLE WITH 2 VOL% SiO_2 SECOND PHASE

Element	TiO_2 (ppmw)
F	0.15
Al	21.3
Cl	50.2
Sc	9.0
V	4.79
Fe	26.2
Ni	8.4
Si	12416.0

carried by Cl impurities to give the conductivity as if for a purer material. The size of the specimen did not influence the measured conductivity.

The conductivities of specimens with dispersions of SiO_2 are shown in Fig. 4 for the two

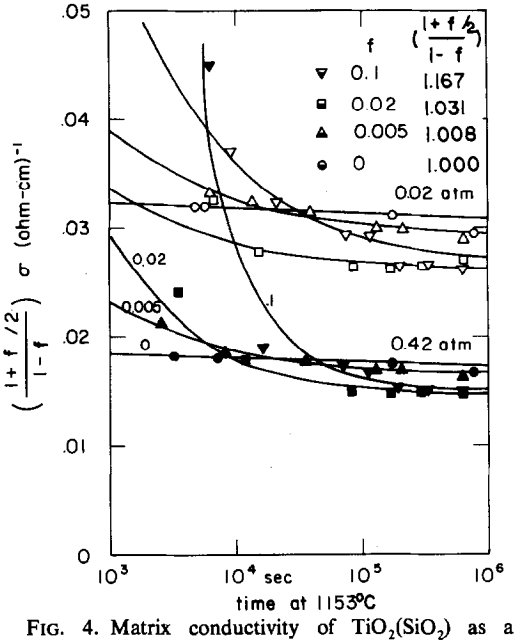

FIG. 4. Matrix conductivity of $TiO_2(SiO_2)$ as a function of time at 1153°C. Each raw datum is multiplied by $(1 + f/2)/(1 - f)$, which is the inverse of the coefficient in Eq. (1). This coefficient accounts for the reduction in conductivity according to classical theory for spherical, insulating particles. The two groups of data are for 0.42 atm = P_{O_2}. The symbols denote ▽ = f = 0.1; □ = 0.02; △ = 0.005; and ○ = 0. The lines are least-squares fits to the data, with parameters given in Table III. The filled symbols denote 0.42-atm O_2 pressure.

partial pressures of oxygen used to generate transients for analysis of chemical diffusivity as a function of the time of annealing. In the figure, each datum has been multiplied by a factor near unity to counteract the expected classical effect (as given below in Eq. (1)) of adding an insulating second phase to a conductive medium. Thus we plot the matrix conductivity, σ_0, rather than the experimentally measured, σ_d. The differences which then remain in the plot are departures from classical two-phase transport. The curves shown are three-parameter fits to the data, in which the last datum in each specimen is taken to be the asymptotic value. The coefficients are listed in Table III. The values are used to obtain interpolated values of conductivity compared to final conductivity for the different specimens at fixed times. In Fig. 5, the highest volume fraction specimen shows the largest increment in conductivity for each of the three interpolated intermediate times.

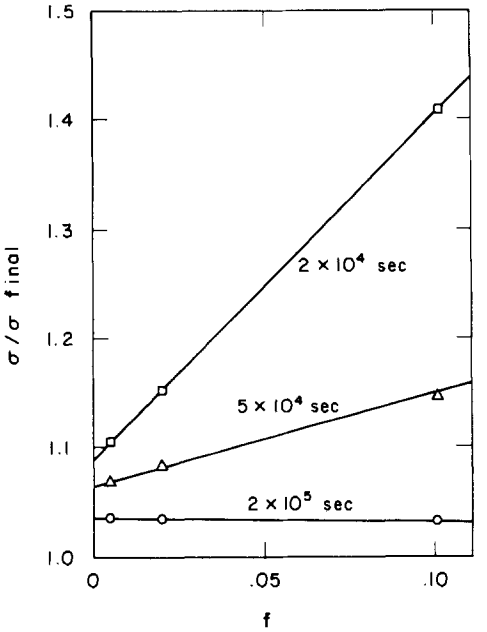

FIG. 5. Conductivity of $TiO_2(SiO_2)$ as a function of volume fraction at fixed times. The ordinate is the value of conductivity interpolated along the least-squares curve divided by the final conductivity of each specimen. The times of anneal are □ = 2 × 10^4 sec; △ = 5 × 10^4 sec; and ○ = 2 × 10^5 sec.

Discussion

The addition of finely divided silica causes marked decreases in the chemical diffusivity and lesser increases in electrical conductivity. With time, the altered properties tend to become more nearly like those of the material without the dispersion. It is apparently a characteristic of the $TiO_2(SiO_2)$ system (notation of Liang (*5*)) for the microstructure to coarsen in the range of times, temperature, and partial pressure of oxygen used here. (For the time-dependent studies the single tem-

TABLE III

COEFFICIENTS FOR THREE-PARAMETER FITS TO DATA SHOWN IN FIG. 4 ACCORDING TO $\sigma(t) = (1 + 10^b t^a)\,\sigma_{final}$

Volume fraction SiO_2	P_{O_2} (atm)	N (number of points)	a	b	σ_{final} $(ohm\text{-}cm)^{-1}$
0.005	0.42	3	−0.4654	1.01	0.01632
	0.02	4	−0.4297	0.823	0.02898
0.02	0.42	6	−0.645	1.95	0.0145
	0.02	6	−0.4831	0.927	0.0260
0.1	0.42	5	−1.09	4.33	0.01509
	0.02	4	0.507	1.07	0.02622

perature 1153°C was used and the atmosphere varied only between 0.02 and 0.42 atm of oxygen.) Changes of properties with time may be related to changes in the dimensions of the microstructure with time and hence can be used to test the consistency of physical and chemical theories to explain the initial effect.

A microstructure which is representative of dispersed phase material during the time of low chemical diffusivity and high electrical conductivity is shown in Fig. 6, which is a transmission electron micrograph of a crushed specimen. Spheres of the second-phase silica as small as 50 Å can be seen. Dark field optical microscopy at 1000 × of a polished cross section showed barely visible bright points with interparticle spacings of less than 3 μm. These points were interpreted as the largest particles in the starting silica powder, and they reflect the high degree of homogeneity in preparation, which is necessary to conclude that the small area observed in a transmission electron micrograph is representative of the whole. After 8 days at temperature, the second-phase thickness can be readily observed optically, though fine grained areas selected preferentially in the TEM preparation reveal particles grown only to 250 Å. The coarse SiO_2 phase seen optically partially wets TiO_2 grain boundaries. The latter structure is shown in Fig. 7. Porosity increases from 2–5 to 5–10% as hot-pressed voids "spring-back." Some of the grains, which were initially 2–5 μm (as measured in fracture and polished cross section), grow to a size 10 times greater. Detailed microstructure data for the 0, 0.5, and 10 vol% specimens are listed in Table IV.

The *classical theory* of conduction and

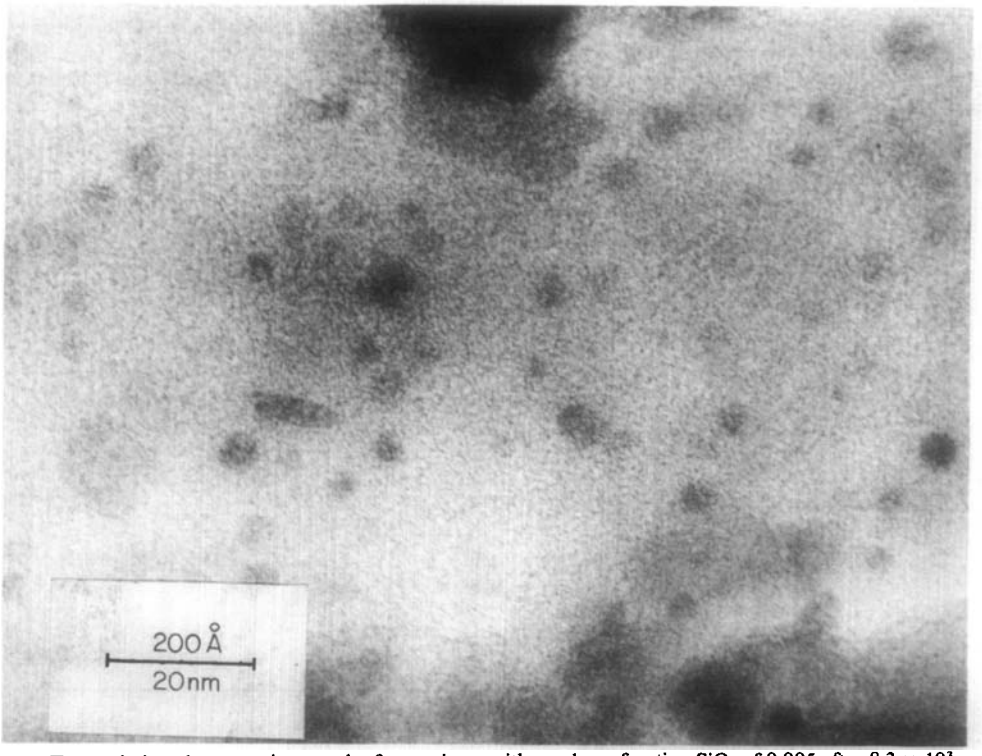

FIG. 6. Transmission electron micrograph of a specimen with a volume fraction SiO_2 of 0.005 after 8.3×10^3 sec at 1153°C. The SiO_2 phase appears as dark spherical objects as small as 50 Å in diameter.

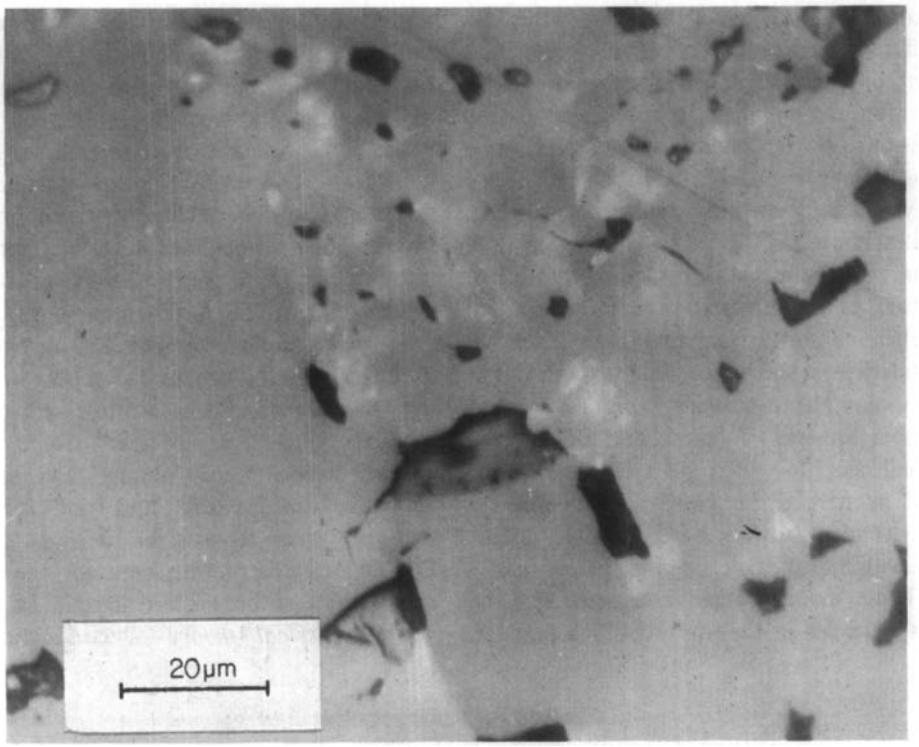

FIG. 7. Reflection optical micrograph of a specimen with a volume fraction of 0.005 SiO_2 at 6.4 × 10^3 sec at 1153°C. The coarse SiO_2 phase appears as light gray angular objects. Variations in the background shading are the result of reflections at grain boundaries below the polished surface.

TABLE IV
MICROSTRUCTURAL MEASUREMENTS OF POROSITY AND SECOND-PHASE DISTRIBUTION

Volume fraction SiO_2	Time at 1153°C (sec)	Apparent volume fraction TiO_2	Grain size (μm)	Average no. of phase boundaries per 100-μm length in planar section	Points per unit volume (cm^{-3})	Mean-free path between particles (μm)
0	7.5×10^3	0.949 ± 0.011	28.2	—	—	—
	8.8×10^5	0.914 ± 0.015	45.9	—	—	—
0.005	8.3×10^3	0.937 ± 0.016	5.0[a]	—	$>2.8 \times 10^{10}$	<3.3
	6.4×10^5	0.852 ± 0.023	28.8[b]	22.8	—	247.0
0.1	2.2×10^4	0.954 ± 0.011[c]	2.0[a]	—	$>1.1 \times 10^{11}$	<2.1
	6.3×10^5	0.868 ± 0.021	32.7[b]	143.4	—	39.3

[a] Determined from fracture surface.

[b] Determined from planar section with nearly crossed Nichols. This technique was not sensitive to finer grains which remained.

[c] The 10 vol% of second-phase particles were too fine to be seen in a light microscope.

diffusion in two-phase mixtures (*3*, *4*) can be expressed for a nonconducting, spherical second phase as

$$\sigma_d = (1 - f)\,\sigma_0/(1 + 0.5f), \qquad (1)$$

where f is the volume fraction of particles, σ_0 is the conductivity of the matrix phase, and σ_d is the conductivity of the dispersed phase mixture. Points: (1) The theory cannot be consistent with the large decrease in $\tilde{D}$. For spherical particles, at least, which are seen in Fig. 6, a decrease of just more than 1.5 times the volume fraction (or 16% with 10 vol% second phase) would be predicted. Decreases are seen to be of the order of 10 times. (2) The classical theory is not consistent with an increase in conductivity with a second, insulating phase. The theory requires that the conductivity of *any* two-phase mixture be intermediate between the properties of the two phases separately. An insulating second phase would not be expected to increase conductivity. (3) It should be noted that at long times, with coarse particle sizes, the classical theory may account for the small differences from dispersion-free materials. As the partially wetting phase seen in Fig. 7 is not spherical, the decreases in conductivity at later times are larger than those calculated for spheres. Thus, differences appear in Fig. 4 in spite of the factor to compensate for the classical spherical particles. Also, one may consider that porosity drives later $\tilde{D}$ values to slightly higher numbers and later conductivities to lower values, in the sense that a pore may be considered a particle with high ion transport (gas phase) and low electron transport.

Solubility of SiO_2 in TiO_2, though known (*15*) to be too small to be detected up to the 1550°C eutectic temperature by X-ray lattice parameter measurements and ir methods, might be an important factor in defect-related transport where ppma quantities can influence properties. Substitutional placement of Si^{4+} for Ti^{4+} would not cause changes in transport on the basis of well-established aliovalent defect models. But the same Si^{4+} ion as an interstitial could displace $Ti_i^{\cdots\cdot}$ interstitials and require a greater electron concentration for electroneutrality. Consequently, a lower $\tilde{D}$ and a higher σ would be observed in the dispersed phase materials. That the solubility would be higher for small particles could account for changes with time. However, there is no reason to find a dependence on volume fraction, as is observed in both $\tilde{D}$ and σ, in Figs. 2, 4 and 5.

The *segregation of impurities* to internal surfaces would leave the remaining matrix material more free of impurities. Consequently, a material with a finely dispersed second phase would have properties which are characteristic of a material purer than the material without the dispersed phase. In particular, the segregation of trivalent cationic impurities such as Fe^{3+} or Al^{3+} to particle surfaces would shift the matrix electroneutrality condition and create more free electrons and fewer $Ti_i^{\cdots\cdot}$ interstitials (or oxygen vacancies) with local chemical equilibrium. In the limiting cases in which the impurity-electron electroneutrality condition prevails, the matrix conductivity σ_0 after dialysis of some, not all, of the impurities to the particle surfaces in a layer of thickness d is approximately

$$\sigma_0 = (1 + 3fr^{-1}\Gamma_0 d/[A]_{total})\,\sigma_b, \qquad (2)$$

where r is the particle radius, Γ_0 is the coverage fraction in the layer of thickness d, and σ_b is the conductivity of a bulk, one-phase crystal doped to the same total impurity level, $[A]_{total}$. For $r = 50$ Å, $(\Gamma_0 d) = 0.5$ Å, volume fraction $f = 0.02$, and $[A]_{total} = 1000$ ppma, we have $\sigma_0/\sigma_b = 1.6$. Clearly, the purer the material, the larger the proportional change after segregation of impurities. The diffusivity, if related to the concentration of ionic defects of opposite sign to the most populous electronic defect, would take a negative sign, rather than a positive sign in Eq. (2). We shall refer to this revised form of Eq. (2) as Eq. (2*). Fine particles would give a lower $\tilde{D}$, through Eq. (2*) and a higher σ, through Eq. (2), for segregation of Fe or Al (but not Cl) impurities to particle surfaces. As the second phase coarsens, either through a regular process or

through the appearance of a new SiO_2 phase, there are fewer sites to which the impurities can segregate; hence a larger fraction must remain in solution, as all must be in the sample with no dispersed phase. (The concentrations of Al and Fe given in Table II are below the solubility limits of these elements.) Thus, with time, the dispersed phase material develops transport properties similar to those of materials without the dispersion. A larger surface area follows from greater volume fractions, and so is consistent with observations here and Eq. (2) and (2*). Presuming a $t^{1/3}$ regular growth law, the change in conductivity would follow a $t^{-1/3}$ law. The observations are close, with exponents of about $-\frac{1}{2}$; see Table III.

Space charge may appear in the vicinity of dispersed particles and shift the equilibrium point defect concentrations. In the absence of impurities, charge can still be transferred to internal surfaces through the process of adsorption. The component shared by both oxide phases, oxygen, may be bound more tightly to one lattice than to the other, as can be indicated by thermal expansion of bonds and by the oxygen activity necessary for dissociation of the oxide. The segregation of charge must be compensated in a volume of the matrix nearby with most of the compensation accomplished in less than a Debye length. Analogous theory applies to the early stages of oxidation in which the thickness of the tarnishing layer is of the order of the Debye length and oxygen is adsorbed at the solid–gas interface (*16*, *17*). An approximate solution for the multiple-defect case has been given by Crosbie (*18*) following a numerical calculation for an electronic defect only by Wagner (*19*). With the sign chosen on the basis of tighter binding of O^{2-} to the TiO_2 phase (thereby yielding a positive charge on the particles and an excess of negative carriers in the matrix), the electrical conductivity of the matrix is approximately

$$\sigma_0 = (1 + 0.83g\,|z|\,f L_D^2/r^2)\,\sigma_b, \qquad (3)$$

where the factor g depends on the surface potential (which is not presently known) and slightly on the geometry of dispersion. Here we can take strong adsorption to mean $g = 20$. The value of L_D is the Debye length of electrostatics and is dependent (as σ_b is) on the bulk defect concentrations as they are controlled, for example, by oxygen partial pressure. The value of z is the charge relative to the lattice of the ionic defect. The diffusivity (again if controlled by a defect of sign opposite to that of the most populous electronic defect) would take a negative sign in Eq. (3). We shall denote that revised form of Eq. (3) as Eq. (3*). Equation (3) is characterized by a linear dependence on volume fraction, f, and an inverse square dependence on particle size, $2r$. For a $t^{1/3}$ particle growth law, the conductivity increment would follow a $t^{-2/3}$ law. The observed value of $t^{-1/2}$ is close; see Table III. Inhomogeneity of the later structure on a scale which can be observed in a light microscope probably prevents a closer numerical analysis by some less approximate model following (*18*). For the diffusivity data, the change is so great that a simple first approximation, involved in derivation of Eq. (3*), ceases to be appropriate for quantitative comparison. The basic features of the data presented here can be explained by the model of Eq. (3) for the conductivity and Eq. (3*) for the diffusivity.

At *grain boundaries*, as well as particle surfaces, impurities or space charge may accumulate. Typically, such boundaries are only considered as high-transport paths because of the higher successful jump frequencies in the region of disorder at a boundary. Here, the lowest $\tilde{D}$'s are observed with the finest grain sizes (both with and without the dispersed phase present). If a space charge of the proper sign appears at the grain boundaries, then the finite thickness of a depleted defect layer would provide a barrier. This would likely hold true even if the grain size were much greater than the Debye length, as the boundaries comprise a continuous net-

work through the solid (as opposed to the dispersed surfaces which were considered with particles above). We may say that there is a certain resistance R to the motion of ions across a single grain boundary extending across a bar specimen cross section. Thus, counting the number of grain boundaries as a function of grain size G, we have

$$\sigma_0^{-1} = \sigma_b^{-1} + RG^{-1} \quad (4)$$

for a specimen of unit length. While increased conductivity and diffusivity by the presence of grain boundaries are well known, we see here that it is possible to get lower transport (either conductivity or diffusivity, separately), depending on the defect which is depleted in a semi-ionic crystal. The case for enhanced and diminished transport by space charge at grain boundaries in purely ionic compounds has been discussed recently by Yan *et al.* (*20*). The fine grain size G accompanies the fine particle size $2r$, so the separation of the effects due to grain boundaries and those due to particles cannot be distinguished in the present experiments.

The common element in each model represented by Eqs. (2)–(4) is the transfer of charged species to internal surfaces. Any one of these three models can explain the strongly altered transport properties which result from the addition of a finely divided second phase.

Conclusion

The effect of a submicron dispersion of SiO_2 on the transport properties of TiO_2 is consistent with three different explanations related to the size of the dispersed particles and the transfer of charge to internal surfaces:

(1) A trivalent impurity segregates to sites on dispersed particle surfaces. Therefore, the impurity does not control the transport in the dispersed phase material in cases in which it would in material without the dispersion. The preferential segregation of Fe and Al (but not Cl) to particle surfaces is an analog for compensating impurities.

(2) The dispersed phase particles take on a positive charge, due to the chemical adsorption of oxygen more strongly to TiO_2 than to SiO_2. Consequently, the particles are surrounded by a space charge layer of excess electronic defects and deficit ionic defect concentrations. For sufficiently small particles the layers nearly overlap.

(3) Grain boundaries are enveloped in space charge layers of excess electronic defects and deficit ionic defect concentrations. The size of the dispersed particles influences the grain size and hence the number of high-transport paths and barrier layers.

A sufficiently small particle size and a sufficiently large volume fraction can cause a lower chemical diffusivity and an increased electronic conductivity, as have been observed in the present experiments. In each of the three explanations, the alteration of concentrations of transport-related point defects occurs as a result of the transfer of charged species to internal surfaces.

The changes of properties with time follow from the same models, as the particle size grows with time and the properties become more like those of material without a dispersed phase. The appearance of a coarse, non-spherical second phase which partially wets grain boundaries is taken to be responsible for decreases in the long-time conductivities which are lower than those predicted by classical theory for spherical particles.

In general, the effect on transport properties of a small volume fraction of submicron oxide particles dispersed in an oxide matrix can be considered in terms of physical and chemical interactions. The physical effects are the basis of small reductions in transport through the classical two-phase theory of Eq. (1) and increases in transport related to grain size through high-transport paths. On these physical bases, the lowest transport is achieved after a dispersoid coarsens, thereby inducing a few large grains to grow and thereby reducing the quantity of high-transport paths.

On the other hand, the chemical effects can

be the basis of large reductions in transport in compound semiconductors, such as oxides, in which the transport properties can be strongly affected by transfer of charge to dispersed particles from the matrix. The chemical equilibrium of the matrix is altered as a result of the transfer of charge (whether this transfer occurs by segregation of dopant ions in Eq. (2) or by the development of a space charge layer in a dopant-free material in Eqs. (3) and (4)). On the chemical basis, the lowest ionic transport and highest electronic transport are to be achieved with the smallest particle sizes, as have been observed here.

It is of interest to note that the Debye length is longest for those oxides which are lowest in ionic defect concentration (native or impurity). In turn, these oxides are the ones with the lowest ion diffusivities in single phases. The addition of a dispersed phase of sufficiently small size can be expected to be the basis of achieving even lower ion diffusivities in polyphase mixtures which have these low-transport oxides as matrix phases.

Acknowledgments

This work was supported by the Materials Research Center of Northwestern University. The author is grateful for a National Science Foundation Graduate Fellowship and a W. P. Murphy Teaching Assistantship. He is indebted to Professor J. B. Wagner, Jr., for his insight and experience in the experimental methods at high temperature and for the suggestion and encouragement to pursue the effect of a dispersed phase. Encouragement from Professors D. L. Johnson and C. Wagner are gratefully acknowledged. Special thanks to S. T. Gonczy for guidance in ceramic hot-pressing.

References

1. I. G. WRIGHT, B. A. WILCOX, and R. I. JAFFEE, *Oxid. Metals* **9**, 275 (1975).
2. C. S. GIGGINS AND F. S. PETTIT, *Met. Trans.* **2**, 1071 (1971).
3. J. CRANK, in "Mathematics of Diffusion," Chap. 12, Oxford Univ. Press (Clarendon), London (1975).
4. R. E. MEREDITH AND C. W. TOBIAS, *Advan. Electrochem. Electrochem. Eng.* **2**, 15 (1962).
5. C. C. LIANG, *J. Electrochem. Soc.* **120**, 1289 (1973).
6. T. JOW, to appear; T. JOW, Ph.D. Thesis, Northwestern University (June 1977).
7. DeGussa, Inc., Pigments Division, 2 Pennsylvania Plaza, New York, N.Y. 10001. Aerosil 130 and 200 and Titanium Dioxide P 25. Note that the numbers 130, 200, and 25 denote the approximate BET surface areas in square meters per gram.
8. J. B. PRICE AND J. B. WAGNER, JR., *Z. Phys. Chem. (N.F.)* **49**, 257 (1966).
9. K. SCHWERDTFEGER AND E. T. TURKDOGAN, *in* "Techniques of Metals Research," Vol. 4, Part 1, p. 321, Wiley, New York (1970).
10. J. F. BAUMARD, to appear. Cited by J. F. BAUMARD, D. PANIS, AND A. M. ANTHONY, *J. Solid State Chem.* **20**, 43 (1977).
11. D. L. VENKATU AND L. E. POTEAT, *Mater. Sci. Eng.* **5**, 258 (1969/70).
12. R. HAUL AND G. DÜMBGEN, *J. Phys. Chem. Solids* **26**, 1 (1965).
13. G. M. CROSBIE, Ph.D. Thesis, Appendix 5, Northwestern University (June 1977).
14. R. N. BLUMENTHAL, J. COBURN, J. BAUKUS, AND W. M. HIRTHE, *J. Phys. Chem. Solids* **27**, 643 (1966).
15. R. C. DEVRIES, R. ROY, AND E. F. OSBORN, *Trans. Brit. Ceram. Soc.* **53**, 531 (1954).
16. R. B. MOSLEY AND A. T. FROMHOLD, *Oxid. Metals* **8**, 19 (1974); **8**, 47 (1974).
17. C. WAGNER, *Corrosion Sci.* **13**, 23 (1973).
18. G. M. CROSBIE, *Corrosion Sci.* **17**, 913 (1977).
19. C. WAGNER, *J. Phys. Chem. Solids* **33**, 1051 (1972).
20. M. F. YAN, R. M. CANNON, H. K. BOWEN, AND R. L. COBLE, *J. Amer. Ceram. Soc.* **60**, 120 (1977).